Blending of Global and Regional Analyses with a Spatial Filter: Application to Typhoon Prediction over the Western North Pacific Ocean

LING-FENG HSIAO,* XIANG-YU HUANG,[+,++] YING-HWA KUO,[+] DER-SONG CHEN,[#] HONGLI WANG,[@,&] CHIN-CHENG TSAI,* TIEN-CHIANG YEH,[#] JING-SHAN HONG,[#] CHIN-TZU FONG,[#] AND CHENG-SHANG LEE*,**

*Taiwan Typhoon Flood Research Institute, National Applied Research Laboratories, Taipei, Taiwan
[+]National Center for Atmospheric Research, Boulder, Colorado
[#]Central Weather Bureau, Taipei, Taiwan
[@]Cooperative Institutes for Research in the Atmosphere, Colorado State University, Fort Collins, Colorado
[&]Global Systems Division, Earth System Research Laboratory, NOAA, Boulder, Colorado
**Department of Atmospheric Sciences, National Taiwan University, Taipei, Taiwan

(Manuscript received 1 May 2014, in final form 27 January 2015)

ABSTRACT

A blending method to merge the NCEP global analysis with the regional analysis from the WRF variational data assimilation system is implemented using a spatial filter for the purpose of initializing the Typhoon WRF (TWRF) Model, which has been in operation at Taiwan's Central Weather Bureau (CWB) since 2010. The blended analysis is weighted toward the NCEP global analysis for scales greater than the cutoff length of 1200 km, and is weighted toward the WRF regional analysis for length below that. TWRF forecast experiments on 19 typhoons from July to October 2013 over the western North Pacific Ocean show that the large-scale analysis from NCEP GFS is superior to that of the regional analysis, which significantly improves the typhoon track forecasts. On the other hand, the regional WRF analysis provides a well-developed typhoon structure and more accurately captures the influence of the Taiwan topography on the typhoon circulation. As a result, the blended analysis takes advantage of the large-scale analysis from the NCEP global analysis and the detailed mesoscale analysis from the regional WRF analysis. In additional to the improved track forecast, the blended analysis also provides more accurate rainfall forecasts for typhoons affecting Taiwan. Because of the improved performance, the blending method has been implemented in the CWB operational TWRF typhoon prediction system.

1. Introduction

Successful numerical prediction of tropical cyclones depends not only on the physical parameterizations of a model but also on the accuracy of the model initial conditions. Several studies have shown that improved model initial conditions through either initialized typhoon vortex structure or data assimilation can improve a typhoon forecast (e.g., Hendricks et al. 2013; Hsiao et al. 2010; Liu et al. 2012).

In regional NWP models, data assimilation techniques such as three-/four-dimensional variational data assimilation (3DVAR and 4DVAR, respectively), ensemble Kalman filter, or the hybrid of these two approaches (Huang et al. 2009; Schwartz and Liu 2014), may improve initial conditions through assimilation of both traditional and special observations. One particular challenge of tropical cyclone prediction is the lack of observations over the ocean. Sizeable systematic biases can accumulate in the initial conditions after a period of continuously cycling data assimilation (e.g., full cycling) because of the lack of observations to correct the first guess, which is based on the model's short-term (e.g., 6 h) forecast (Hsiao et al. 2012). The accumulation of systematic errors in the initial conditions would significantly impact the performance of a tropical cyclone prediction model.

Another challenge for regional data assimilation is the existence of lateral boundaries. Since observations

[++] Current affiliation: Centre for Climate Research Singapore, Meteorological Service Singapore, Singapore.

Corresponding author address: Dr. Ling-Feng Hsiao, Taiwan Typhoon Flood Research Institute, National Applied Research Laboratories, 11F, No. 97, Sec. 1, Roosevelt Rd., Taipei 10093, Taiwan.
E-mail: lfhsiao@gmail.com

DOI: 10.1175/WAF-D-14-00047.1

outside the regional model boundaries would not have an influence on the analysis inside the model domain, the quality of analysis near the model lateral boundaries would be degraded. Depending on the scale length of the background error covariance, the influence could reach several thousand kilometers into the interior of the model domain. As a result, the large-scale aspect of a regional analysis is inferior to that of a global analysis, which suffers no boundary effects. One possible approach to remedy this problem is to use the global analysis as the first guess in a partial cycling data assimilation procedure to suppress the growth of the analysis error (Hsiao et al. 2012).

Another approach to improve the quality of the initial conditions is the use of a blending technique (Durand and Bougeault 1987; Ajjaji and Issara 1994; Brožkovà et al. 2001; Yang 2005). Durand and Bougeault (1987) proposed a spectral interpolation approach to merge the global analysis with the regional analysis from a limited-area model (LAM) of Météo-France. Ajjaji and Issara (1994) also proposed a method for mixing the LAM and the global model data in gridpoint space. Brožkovà et al. (2001) adopted a different approach, which combines the spectral and gridpoint data from global and regional analyses with the use of a digital filter. Yang (2005) used an incremental spatial filter to blend the large-scale analysis from the European Centre for Medium-Range Weather Forecasts (ECMWF) with the small-scale fields from the High Resolution Limited Area Model (HIRLAM). His blending method has been operational at the Danish Meteorological Institute since 2006. Given the deficiency in the large-scale aspect of a regional analysis, the use of large-scale information from a global analysis may improve the regional model forecasts (Guidard and Fischer 2008; Dahlgren and Gustafsson 2012).

Taiwan's Central Weather Bureau (CWB) implemented a Typhoon WRF (TWRF) regional forecast system in 2010, which includes a partial cycling analysis procedure based on the WRF three-dimensional variational data assimilation system. Even though partial cycling has been effective in suppressing the growth of systematic regional model errors, significant bias over the ocean remains (Hsiao et al. 2012; see their Fig. 12). One important source of TWRF regional analysis error is the absence of satellite radiance assimilation, which can be quite important over the ocean. To reduce the error for the TWRF Model initial conditions, we adopt the blending technique from Yang (2005) to merge the large-scale analysis from NCEP GFS with the regional analysis of TWRF. We take this approach with the following consideration: (i) a global data assimilation system can assimilate more observations (particularly, the satellite radiance observations) and provide a better large-scale analysis than a regional data assimilation system can (for the reasons mentioned earlier); (ii) NCEP GFS uses more nontraditional meteorological data than the CWB operational system; moreover, the performance of NCEP GFS has been significantly improved recently with the use of hybrid variational–ensemble data assimilation (Wang et al. 2013); and (iii) a regional cycling data assimilation may produce more accurate small-scale analyses with the use of high-resolution model forecasts as the background and the assimilation of local observations, which may not be used by NCEP GFS (Schwartz and Liu 2014).

In this paper, we assess the impact of the blending technique on the prediction of 19 typhoons from July to October 2013 over the western North Pacific Ocean. This study is the first application of the blending technique for the operational prediction of tropical cyclones over the western North Pacific. Section 2 provides a detailed description of the model, the blending method, and the experiment design. Forecast results from partial cycling, the blending technique, and NCEP GFS initial conditions are discussed in section 3. The conclusions are given in section 4.

2. Model configurations and experimental design

a. The TWRF modeling system

The TWRF is based on the nonhydrostatic Advanced Research version of WRF (ARW; Skamarock et al. 2008) with a triple-nested domain (Fig. 1). The horizontal grid spacing was 45 km (221 × 127 grid points) for the outermost domain, 15 km (183 × 195 grid points) for the middle domain, and 5 km (240 × 192 grid points) for the inner domain. One-way interactive nesting is used with the nested domains. Forty-five vertical levels are used in each domain with more levels concentrated in the lower troposphere.[1] The TWRF uses the following physics options: the Goddard microphysics scheme (Tao et al. 2003), the Kain–Fritsch cumulus parameterization scheme (Kain and Fritsch 1990), the Yonsei University (YSU) planetary boundary layer scheme (Hong et al. 2006), the Noah land surface model (Chen and Dudhia 2001), and the Rapid Radiative Transfer Model for Global Climate Models (RRTMG; Mlawer et al. 1997; Iacono et al. 2008) longwave and shortwave radiation schemes.

The analysis component of TWRF is based on the WRF 3DVAR system (Barker et al. 2004). The WRF

[1] The 45 vertical levels with sigma values in the terrain-following coordinate are 1.0, 0.995, 0.988, 0.98, 0.97, 0.96, 0.945, 0.93, 0.91, 0.89, 0.87, 0.85, 0.82, 0.79, 0.76, 0.73, 0.69, 0.65, 0.61, 0.57, 0.53, 0.49, 0.45, 0.41, 0.37, 0.34, 0.31, 0.28, 0.26, 0.24, 0.22, 0.2, 0.18, 0.16, 0.14, 0.12, 0.1, 0.082, 0.066, 0.052, 0.04, 0.03, 0.02, 0.01, and 0.0.

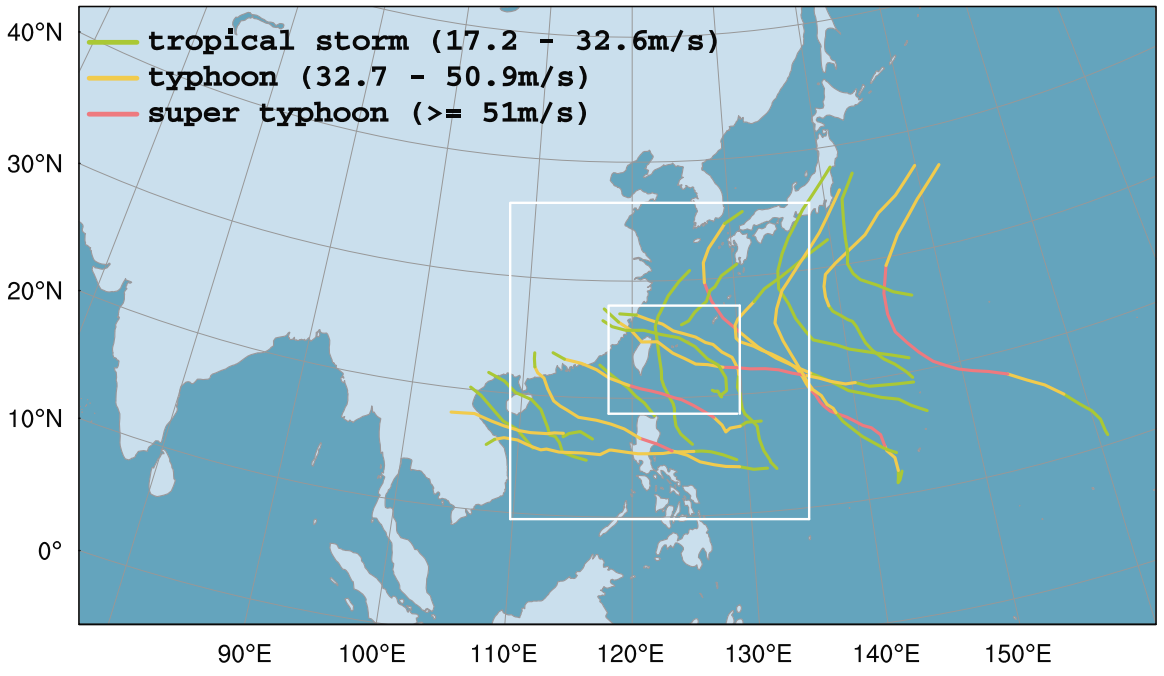

FIG. 1. Domain of the triple-nested TWRF and typhoon tracks based on CWB best tracks of 19 typhoons from July to October 2013 over the western North Pacific Ocean. The lines indicate the track for each typhoon during its life cycle. Colors of different segments of the track designate the storms at different stages.

3DVAR uses an incremental formulation to produce multivariate incremental analyses for surface pressure, wind, temperature, and relative humidity at the model grid points. The minimization of the incremental cost function is conducted in a preconditioned control variable space. The "cv5" option, used in this study, formulates the background error statistics in terms of physical-space control variables including streamfunction, unbalanced velocity potential, unbalanced surface pressure, unbalanced temperature, and "pseudo" relative humidity.

The observations used by the WRF 3DVAR include synoptic (SYNOP; surface pressure, temperature, wind, and relative humidity), buoys (BUOY; surface pressure, temperature, wind, and relative humidity), METARs (wind and temperature), Quick Scatterometer (QuikSCAT; surface wind), ships (SHIP; surface pressure, temperature, wind, and relative humidity), aviation reports (AIREP; wind and temperature), pilot reports (PILOT; wind), soundings (SOUND; surface pressure, temperature, wind, and relative humidity), GPS radio occultation (refractivity), GPS zenith total delay (ZTD), geosynchronous atmospheric motion vectors (GEOAMV; wind), and satellite temperature (SATEM; temperature). We use three outer loops and the partial cycling option, which are found to be optimal for TWRF application (Hsiao et al. 2012). The partial cycling begins with a cold start that is based on the NCEP GFS analyses at 0.5° resolution, followed by two update cycles using the 6-h WRF forecasts from the previous cycle as the first guess. Meanwhile, the typhoon vortex initialization procedure of Hsiao et al. (2010), which includes vortex relocation, is utilized to minimize the typhoon position error in the first guess. Because of the lack of real-time mesoscale observations (such as airborne radar observations) near the inner core of tropical cyclones over the western North Pacific Ocean, it is difficult for the WRF 3DVAR to provide a realistic initial vortex with detailed, accurate mesoscale structure. However, a vortex with better dynamic balance could be generated through the WRF 3DVAR partial cycling (Hsiao et al. 2012).

b. *Blending method*

The blending method used in this study is based on an incremental spatial filtering scheme proposed by Yang (2005). The resulting analysis, which combines the large-scale analysis from NCEP GFS and the small-scale analysis from TWRF is defined as

$$\mathrm{TWRF}_{\mathrm{bld}} = \mathrm{TWRF}_{\mathrm{ana}} + \overline{\mathrm{NCEP\,GFS}_{\mathrm{ana}}}^{\mathrm{sf}} - \overline{\mathrm{TWRF}_{\mathrm{ana}}}^{\mathrm{sf}}, \tag{1}$$

where bld, ana, and sf designate the blended model state, analysis state, and a low-pass spatial filter. We adopt the sixth-order tangent implicit filter here, which

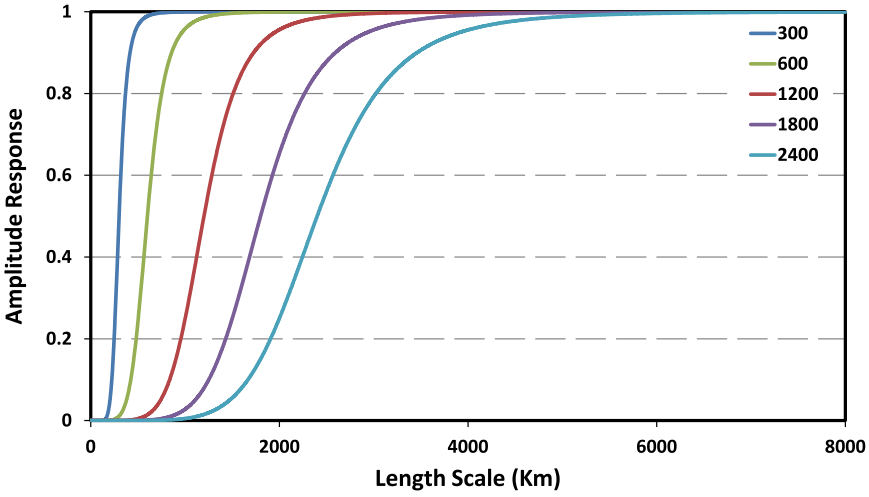

FIG. 2. Amplitude responses of a sixth-order tangent implicit filter from Raymond and Garder (1991) for cutoff lengths of 300, 600, 1200, 1800, and 2400 km, respectively.

is described by Raymond and Garder (1991), and the amplitude response $H(L)$ is defined as

$$H(L) = [1 + \varepsilon \tan^6(\pi \delta x/L)^{-1}], \quad (2)$$

where L is the length scale and the filter parameter ε can be calculated as

$$\varepsilon = \tan^{-6}(\pi \delta x/L_x), \quad (3)$$

where δx is the grid spacing and L_x is the cutoff length scale. Figure 2 shows the different cutoff length of 300, 600, 1200, 1800, and 2400 km with a low-pass spatial filter in the form of an amplitude response. In a way, the curve represents how the blending method combines TWRF (left of the curve) and NCEP GFS (right of the curve) analyses into a new analysis. Note that at the cutoff length, the contributions from the two respective analyses are exactly evenly divided. We have tested different choices of cutoff length, including 300, 600, 1200, 1800, and 2400 km, and found that the 1200-km cutoff length gave the best performance (not shown). Moreover, Hsiao et al. (2010) showed that the 1200-km cutoff length is a good choice to separate small-scale circulation patterns from the environmental flow. Based on these results, we select 1200 km as the cutoff length with the blending procedure in this paper. We realize, of course, that the optimal choice of the cutoff length may change, depending on the relative quality of NCEP GFS and the regional WRF analyses at different scales.

The blending is applied to wind, potential temperature, water vapor mixing ratio, and pressure as in Eq. (1). Because the hydrostatic dry surface pressure and geopotential height are diagnostic variables in the WRF Model, they should be diagnosed from potential temperature, water vapor mixing ratio, and surface pressure (Skamarock et al. 2008). In other words, once the potential temperature, water vapor mixing ratio, and pressure are modified, the hydrostatic dry surface pressure and geopotential height should be recalculated to prevent the WRF initial state from becoming unbalanced, as discussed in Hsiao et al. (2010).

c. *Experimental design*

In this paper, we test a blended analysis for the purpose of initializing the TWRF Model, which has been in operation at CWB since 2010. To assess the impact of the blending method, we perform three sets of experiments with model initial conditions obtained from partial cycling analysis (PAR; Hsiao et al. 2012), blended analysis (BLD), and NCEP GFS analysis (GFS), for a total of 19 typhoons (279 cases) from July to October 2013 over the western North Pacific Ocean. Note that the partial cycling is applied to all three (45, 15, and 5 km) of the model domains. The tracks and storm information for these 19 typhoons are shown in Fig. 1 and Table 1, respectively. (Tabulations of the 6-hourly best-track positions and intensities can be found on the CWB website, which is available online at http://rdc28.cwb.gov.tw/data.php.) The dates given in Table 1 include the stage from a named tropical storm to a depression 24 h prior (to ensure that track forecast length is at least 24 h for verification). These 19 events consisted of eight tropical storms, five typhoons, and six super typhoons. It is worth noting that Supertyphoon Soulik, the only storm that made landfall on Taiwan, produced strong wind and heavy rainfall over Taiwan (Fig. 1).

TABLE 1. Statistics of 19 typhoons from July to October 2013 over the western North Pacific Ocean.

Typhoon	Forecast period	Intensity	Movement	Case No.
Soulik	0000 UTC 8 Jul–1800 UTC 12 Jul	Supertyphoon	Westward	20
Cimaron	0000–1200 UTC 17 Jul	Tropical storm	Northward	3
Jebi	0000 UTC 31 Jul–0600 UTC 2 Aug	Tropical storm	Westward	10
Mangkhut	1200–1800 UTC 6 Aug	Tropical storm	Westward	2
Utor	1800 UTC 9 Aug–0600 UTC 14 Aug	Supertyphoon	Westward	19
Trami	0000 UTC 18 Aug–0600 UTC 21 Aug	Tropical storm	Recurved	14
Kong-Rey	0600 UTC 26 Aug–1200 UTC 29 Aug	Tropical storm	Recurved	14
Toraji	1800 UTC 1 Sep–1800 UTC 2 Sep	Tropical storm	Northward	5
Man-Yi	0000 UTC 13 Sep–0600 UTC 15 Sep	Tropical storm	Recurved	10
Usagi	1800 UTC 16 Sep–0000 UTC 22 Sep	Supertyphoon	Westward	19
Pabuk	0600 UTC 21 Sep–1800 UTC 25 Sep	Typhoon	Recurved	18
Wutip	0600 UTC 27 Sep–0000 UTC 29 Sep	Typhoon	Westward	8
Sepat	0000 UTC 30 Sep–1200 UTC 1 Oct	Tropical storm	Recurved	7
Fitow	1200 UTC 30 Sep–0000 UTC 6 Oct	Typhoon	Recurved	23
Danas	0600 UTC 4 Oct–1800 UTC 7 Oct	Supertyphoon	Westward	15
Nari	1200 UTC 9 Oct–0600 UTC 14 Oct	Typhoon	Westward	20
Wipha	1800 UTC 10 Oct–0000 UTC 15 Oct	Typhoon	Recurved	18
Francisco	1200 UTC 16 Oct–0000 UTC 25 Oct	Supertyphoon	Recurved	35
Lekima	1800 UTC 20 Oct–0600 UTC 25 Oct	Supertyphoon	Recurved	19

3. Experimental results

a. Impact on track forecasts

For all practical purposes, the track forecast is most important for typhoon prediction in Taiwan. This is because the typhoon rainfall distribution over Taiwan is strongly modulated by the Central Mountain Range (CMR). Accurate forecasts of typhoon track provide a reasonable estimate of rainfall amounts and their distribution through various dynamic and statistical methods. For these reasons, we focus the impact of our analysis blending on track forecast. The verification is performed against CWB best-track data only for the time periods listed in Table 1. The comparison of

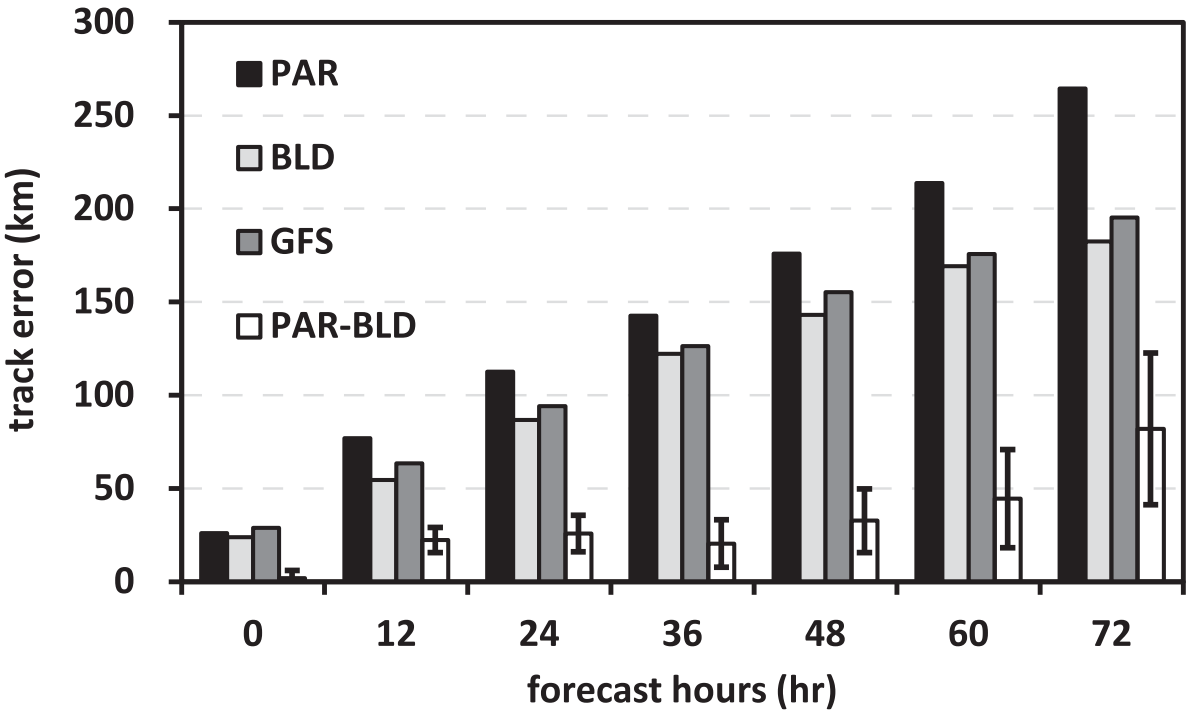

FIG. 3. Mean typhoon track errors for the PAR (black bars), BLD (light gray bars), and GFS (dark gray bars) experiments. Error bars denote the 95% confidence interval of the mean difference between PAR and BLD (PAR − BLD, white bars).

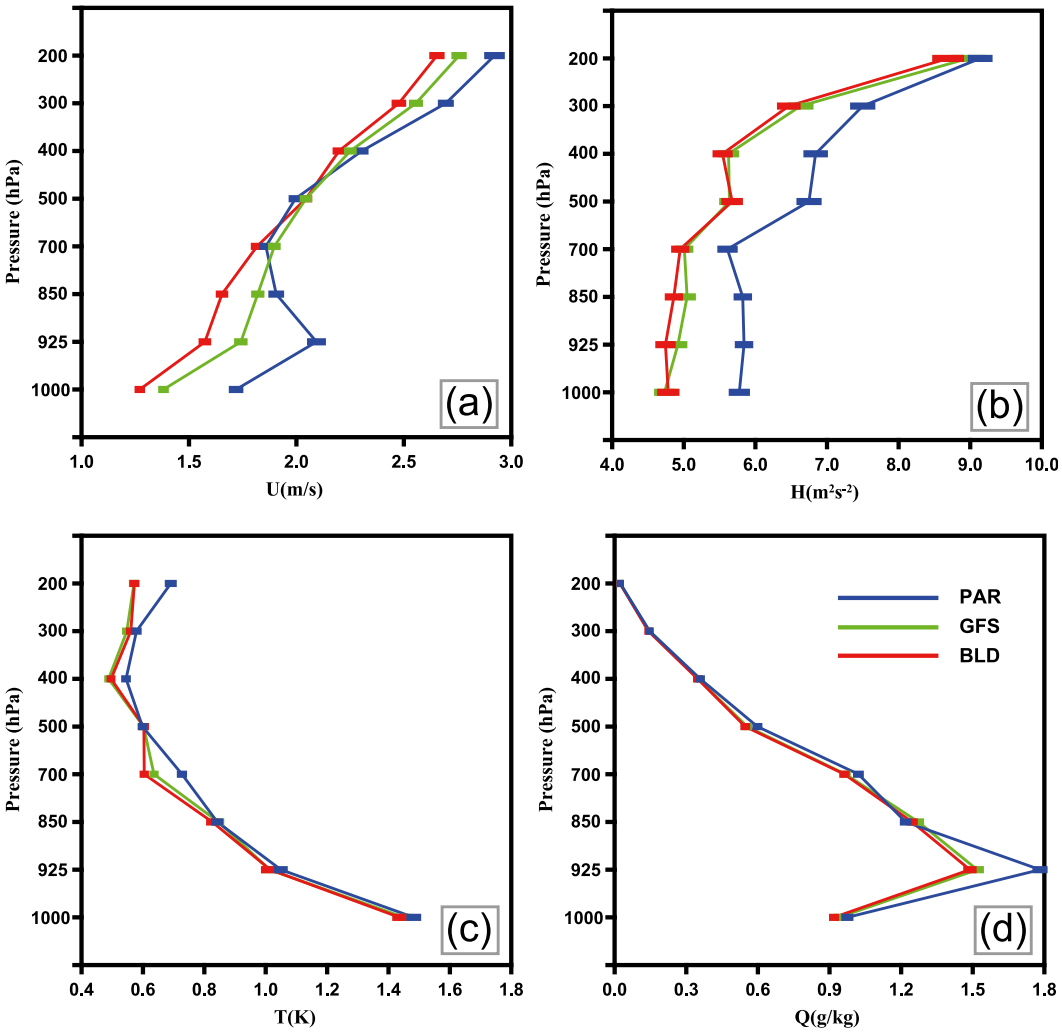

FIG. 4. Vertical profile of the analysis RMSEs of (a) U, (b) H, (c) T, and (d) Q for three experiments. Horizontal error bars denote the 5% and 95% percentiles determined from bootstrap resampling.

the mean track errors for the 45-km domain between the PAR and BLD experiments clearly shows much improved typhoon track forecasts with the blended analysis (Fig. 3). Because all experiments employ a vortex relocation scheme to move a typhoon from its analyzed position to the observed location (based on CWB subjective analysis), there is no large difference at the initial time. The superior performance of the BLD run to the PAR run is evident throughout the entire 72-h forecast period.

We perform a Student's t test to assess the statistical significance of the differences in track error between PAR and BLD, using the 95% confidence interval as the significance delimiter. The vertical bar in Fig. 3 denotes the 95% confidence interval of the mean difference between PAR and BLD. If the interval does not intercept zero, the difference is statistically significant at the 95% confidence level. The results show that the differences between PAR and BLD are statistically significant at the 95% confidence level throughout the 72-h forecast. This implies that the improvement over partial cycling on typhoon track forecasts using BLD is statistically significant. The reduction in track forecast error is as much as 80 km at 72-h forecast, a 30% improvement over PAR.

Figure 3 also compares the 45-km WRF experiment initialized from the NCEP GFS analysis with that of the blended analysis. The difference in track forecast between the BLD and GFS experiments is not more than 15 km for the entire 72-h forecasts, with BLD performing slightly better than GFS. However, the Student's t test is not statistically significant between these two experiments. Since the environmental steering is the most important factor influencing the typhoon movement (Anthes 1982; Chan and Gray 1982), the accuracy of the

track forecasts critically depends on the accuracy of the large-scale flow. Therefore, it is not surprising that the track forecast using BLD is similar to that of GFS analysis (GFS), with the blended analysis giving slightly better performance.

b. *Verification against ECMWF analysis*

Another approach to evaluating the quality of the blended analysis is to verify it against an independent analysis. For this purpose, we compare the PAR, BLD, and GFS analyses against the high-resolution ECMWF operational analysis, which has a horizontal resolution of approximately 25 km. The RMSE of horizontal winds U, geopotential height H, temperature T, and the mixing ratio of water vapor Q are calculated between the model analyses and the ECMWF analyses at 0000, 0600, 1200, and 1800 UTC each day over the 45-km model domain for the 19 typhoon cases. The statistical significance of the RMSE results is established using a bootstrap resampling method (Wilks 1997), whereby the distribution is resampled 10 000 times and the 90% confidence bounds are considered meaningful herein.

Figure 4 shows the vertical profiles of the mean RMSE of the analysis of U, H, T, and Q averaged over all cases for the three analyses. The results show that the RMSE of BLD is generally significantly smaller than that of PAR for all variables. The difference between BLD and PAR in geopotential height is particularly noticeable (Fig. 4b). This indicates that partial cycling after two update cycles using a 6-h WRF forecast as the first guess could produce sizeable systematic model error, particularly in geopotential height. By comparison, the temperature, mixing ratio of water vapor, and horizontal wind all have relatively smaller model errors compared with geopotential height. The geopotential height is a diagnostic variable calculated from the potential temperature, water vapor mixing ratio, and surface pressure in the WRF Model; therefore, the forecast error of the geopotential height is a reflection of the accumulation of errors in these variables. The differences between BLD and GFS among all the variables are not statistically significant, except for horizontal wind and a few levels in geopotential height. These results are consistent with the typhoon track verification.

To gain further insight, we also examine the spatial distribution of the analysis differences of these three experiments from the ECMWF global analysis. Hsiao et al. (2012) showed that although the partial cycling was effective in reducing the systematic warm bias of full cycling, sizeable temperature errors remain over the ocean where there are few traditional observations (see their Fig. 12, which shows the temperature bias at 700 hPa). This warm bias can be partially attributed to the lack of satellite radiance assimilation in TWRF. Here, we compare the temperature difference at 700 hPa between the three analyses and the ECMWF analysis averaged over the 19 typhoons (Fig. 5).

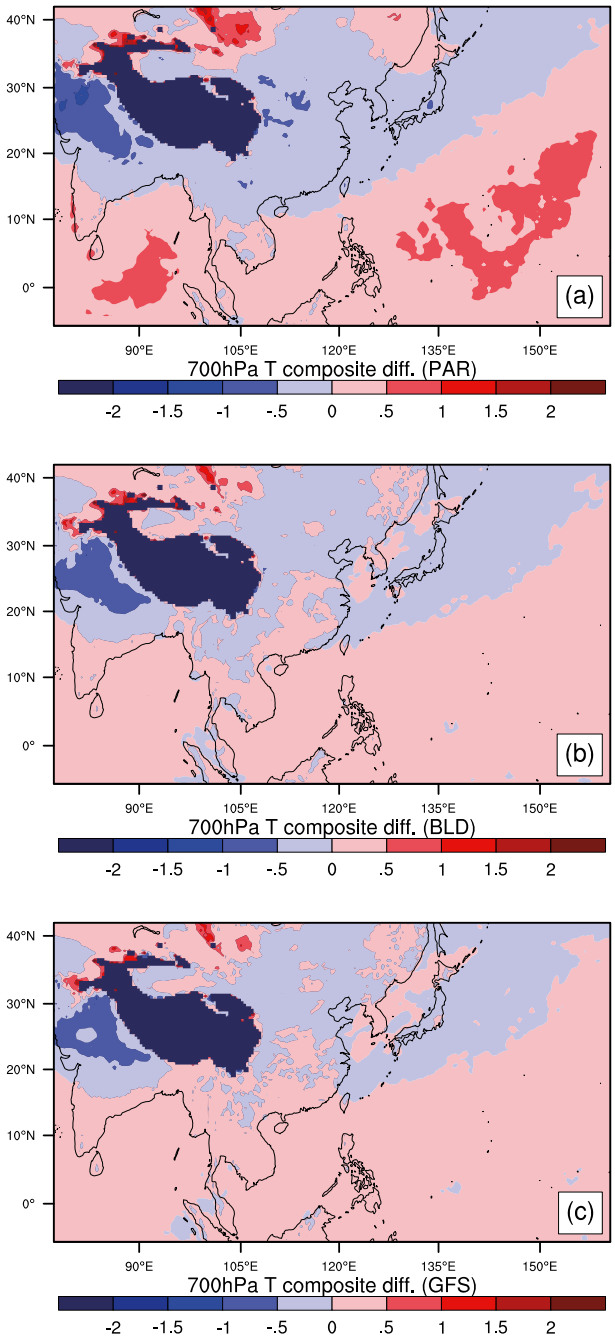

FIG. 5. The differences between the composite analyses of the (a) PAR, (b) BLD, and (c) GFS experiments and ECMWF from 19 typhoons for temperature (°C) at 700 hPa.

If we regard the ECMWF analysis as the "truth," PAR has a clear systematic warm bias over the western North Pacific and the Indian Ocean. For BLD, the

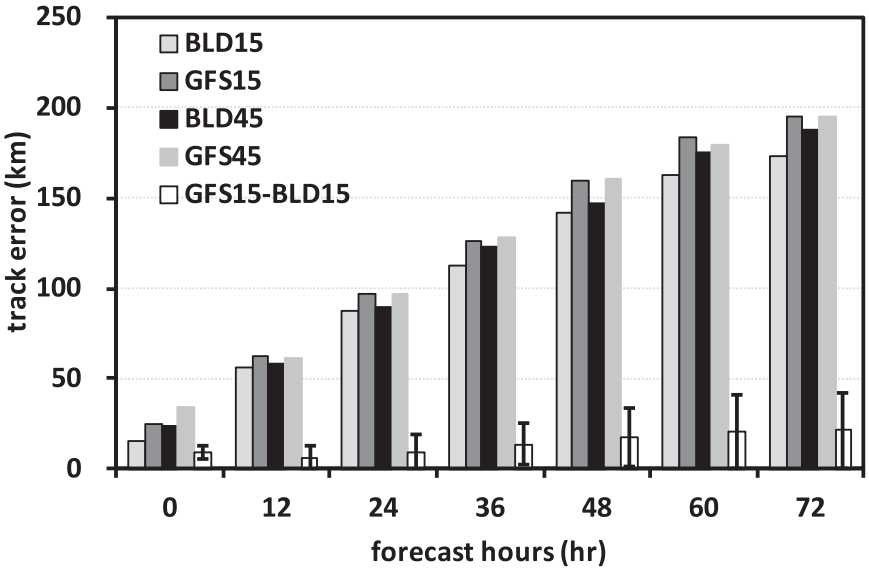

FIG. 6. Comparison of mean track errors between 45- and 15-km resolutions in the BLD and GFS experiments for a total of 143 cases within the 15-km domain. Error bars denote the 95% confidence interval of the mean difference for 15-km resolution between GFS and BLD (GFS − BLD, white bars).

systematic warm bias disappeared over the ocean. The GFS analysis has a similar difference compared to that of the blended analysis, when verified against the ECMWF analysis. These results suggest that the systematic errors in PAR are dominated by large-scale errors and are, primarily, caused by the TWRF Model forecasts (which are used as a first guess in the cycling analysis). There are two possible sources of errors. First, because of the existence of lateral boundaries, observations outside the model domain would not have an influence on the analysis inside the model domain through data assimilation. Second, without the assimilation of satellite radiance data, the partial cycling has limited ability to remove the warm bias developed by the TWRF Model. With PAR on scale greater than 1200 km (the cutoff length) replaced by that of the NCEP GFS analysis, the large-scale errors are largely eliminated in BLD.

The above results show that the blending method is effective in correcting the large-scale analysis of partial cycling by replacing it with that of the NCEP GFS analysis. As a result, the accuracy of the overall analysis is improved and the typhoon track errors are significantly reduced. The advantage of BLD over GFS is that it retains the small-scale features of the regional analysis. One key question is: Does PAR offer more accurate small-scale analysis and, if so, does it benefit the forecast? To answer this question, the high-resolution (15-km grid) forecasts are evaluated to assess the advantages of the blended analysis over the GFS analysis.

c. *High-resolution results*

1) 15-KM TRACK FORECASTS

We compare the mean track errors for the 15-km domain (Fig. 6), which includes a total of 143 cases, approximately half the number found in the 45-km domain (279 cases). The Student's *t* test shows that the differences between BLD and GFS are statistically significant at the 95% confidence level for the 15-km domain (Fig. 6). It is interesting to note that the TWRF initialized with the NCEP GFS model has very similar performance over both the 15- and 45-km grids. This is to be expected as the TWRF analysis on both the 15- and 45-km grids are interpolated from the same NCEP GFS analysis. However, the 15-km blended analysis benefits from the partial cycling analysis on the 15-km grid. The first guess for partial cycling is the 6-h TWRF forecast on the 15-km grid, which contains useful mesoscale information and is dynamically consistent with the topography of the 15-km grid. As a result, the performance of the blended analysis is different between the 15- and 45-km grids, with the 15-km domain yielding better performance. The benefit of blending is clearly evident, as the blended analysis can take advantage of the detailed mesoscale analysis on the 15-km grid produced by partial cycling analysis. Indeed, the blended analysis has the best of both worlds: superior large-scale analysis from NCEP GFS and detailed mesoscale analysis from the partial cycling, which gives the best-track forecasts on both the 45- and 15-km grids. Next, we examine the rainfall prediction and mesoscale

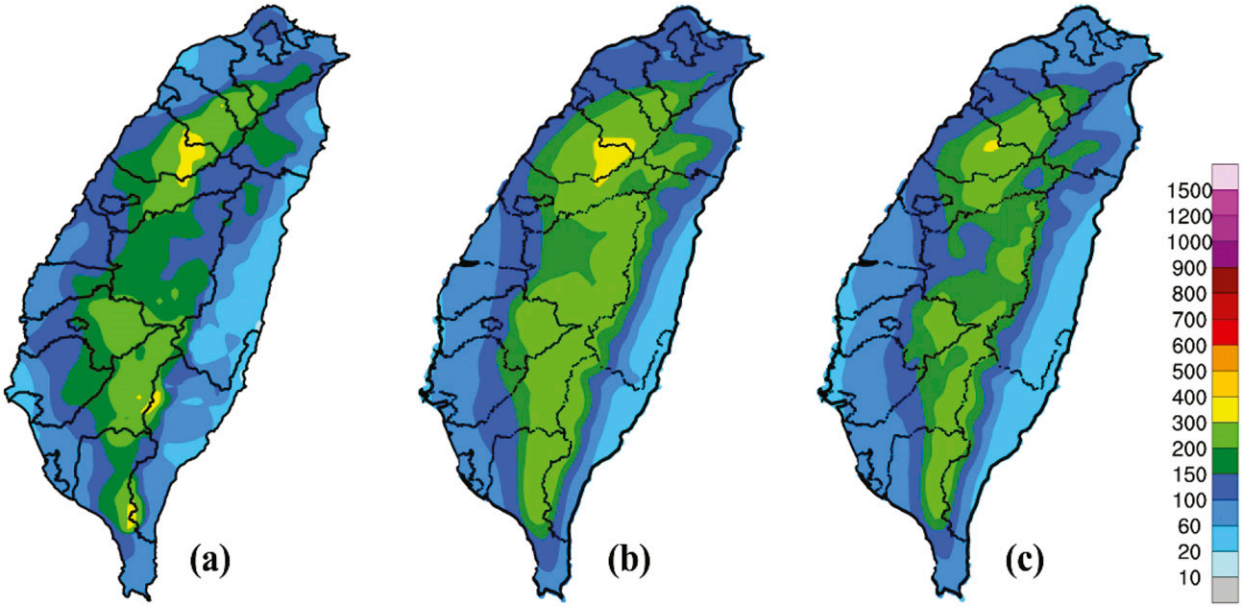

FIG. 7. The 24-h accumulated rainfall composites from the five typhoons (Trami, Kong-Ray, Soulik, Fitow, and Usagi) for (a) observed rainfall and the (b) BLD, and (c) GFS experiments.

structure for Typhoon Soulik between the BLD and GFS experiments within the 5-km inner domain.

2) RAINFALL PREDICTION

Typhoon rainfall is responsible for most of the damage caused by approaching typhoons in Taiwan and is, therefore, the highest priority for typhoon prediction at Taiwan's Central Weather Bureau. Thus, we selected Typhoons Trami, Kong-Ray, Soulik, Fitow, and Usagi, which approached Taiwan and produced heavy rainfall during 2013, to evaluate the five-typhoon composite rainfall between the BLD and GFS experiments (Fig. 7). The maximum 24-h accumulated rainfall produced by the five-typhoon composite is located over the mountainous northwestern area of the country. The forecasts from the GFS and BLD experiments both place the maximum 24-h rainfall at the correct location (Figs. 7b and 7c). The BLD experiment accurately captures the maximum rainfall amount over northwestern Taiwan, while the GFS experiment underpredicts the maximum rainfall amount. The equitable threat score (ETS) and bias score (BS) are calculated for 24-h accumulated rainfall forecasts at various thresholds for the five-typhoon composite, using the Kriging technique (Hsiao et al. 2013), and are shown in Fig. 8. The ETS for the BLD experiment exceeds 0.4, except at the 10-, 300-,

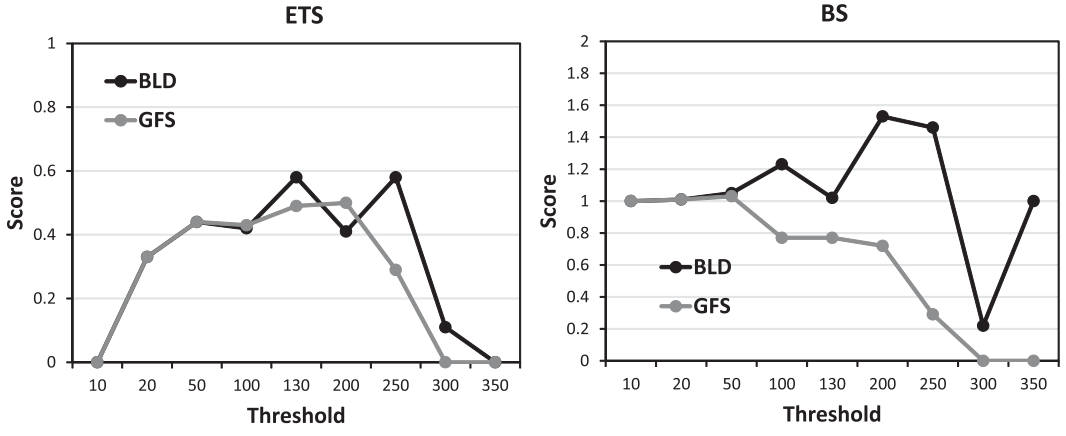

FIG. 8. The (left) ETS and (right) BS with various thresholds (mm) for a 24-h accumulated rainfall forecast composite of five typhoons (Trami, Kong-Ray, Soulik, Fitow, and Usagi).

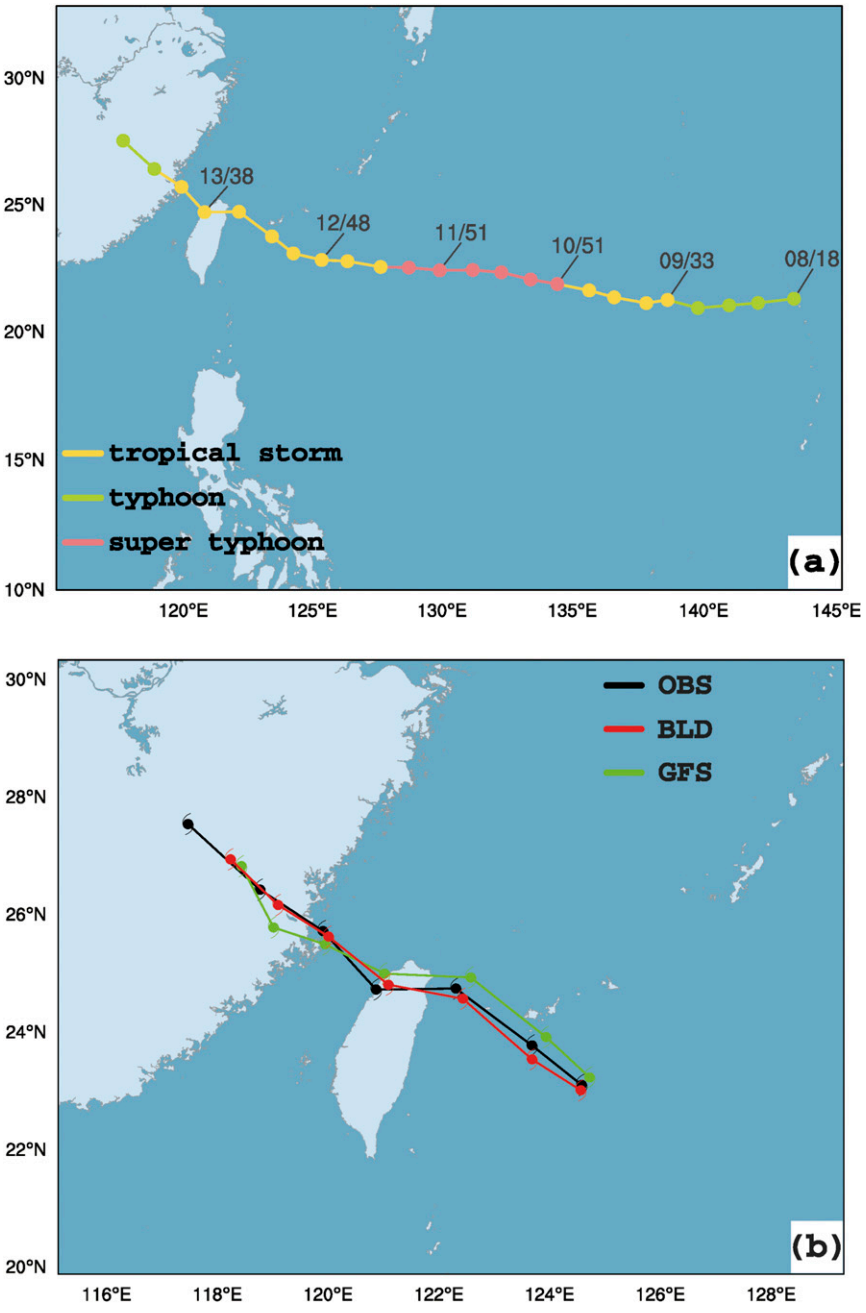

FIG. 9. (a) Tracks of Typhoon Soulik plotted every 6 h from the CWB best track with labels indicating the date during July 2013 of the 0000 UTC position. The maximum surface wind speed ($m\,s^{-1}$; from CWB) is also indicated. (b) The CWB best track (black), BLD (red), and GFS (green) experiments for a 72-h forecast starting at 0600 UTC 12 Jul 2013.

and 350-mm thresholds. As expected, BLD yields better rainfall forecasts than does the GFS experiment except for the 200-mm threshold. In general, BLD also performs better than GFS in terms of BS. The BLD experiment tends to overforecast and the GFS experiment tends to underforecast rainfall. Overall, the blended analysis better captures the topographic effects of the Central Mountain Range and produces a better rainfall forecast.

3) TYPHOON SOULIK: A CASE STUDY

To gain further insight into the impacts of the blending method, we now analyze the mesoscale feature and its associated rainfall prediction between the BLD and

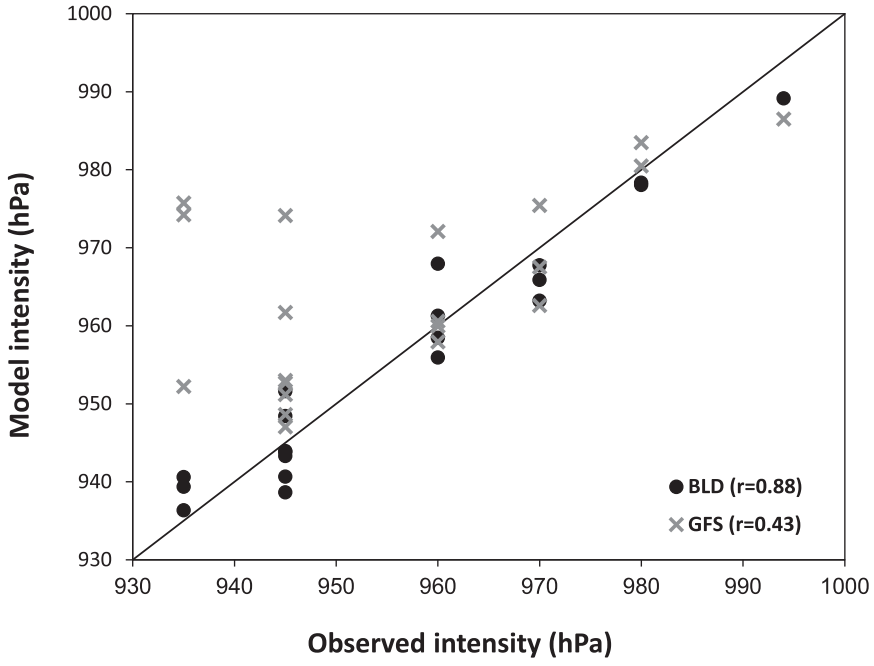

FIG. 10. Scatterplots of model intensity (*y* axis) against the observations (*x* axis) for the BLD and GFS experiments. The solid black line represents the 45° line with the values above (below) indicating the underprediction (overprediction) of storm intensity.

GFS experiments on Typhoon Soulik as a case study. During 2013, Typhoon Soulik was the only typhoon that made landfall on Taiwan, which produced heavy rainfall and caused significant agricultural and industry damage, as well as loss of life. Soulik became a tropical storm to the north of Guam at 0000 UTC 8 July 2013 and moved west-northwestward after reaching super-typhoon intensity (Fig. 9a). A scatter diagram of model intensity versus observed intensity for BLD and GFS, which can be used to evaluate the performance of the intensity forecast for a typhoon approaching Taiwan, is shown in Fig. 10. For GFS, most of the points are located around the top left of the diagonal line, indicating that the forecasted typhoon intensity is generally weaker than the observed intensity, particularly for strong typhoons. For the BLD experiment, points are generally distributed along the diagonal line with a correlation coefficient of 0.88. The low correlation of 0.43 for the GFS experiment indicates relatively poor performance in typhoon intensity forecasts. Therefore, the blending method does indeed provide a better intensity forecast for the Typhoon Soulik case.

Soulik made landfall at about 1800 UTC 12 July at I-lan in northeastern Taiwan and then rapidly weakened and crossed over northern Taiwan. We select the forecast initialized at 0600 UTC 12 July as an example. For the ensuing 36-h period, Typhoon Soulik affected Taiwan and caused severe damage. We will focus on the comparison of the blended analysis and GFS analyses in terms of typhoon structure and their impact on rainfall forecasts within the 5-km domain.

Figure 9b shows the best track of Typhoon Soulik as well as the 36-h track forecast from the blended and NCEP GFS analyses. The predicted tracks from the BLD and GFS experiments follow closely with the observed track, with that of BLD giving slightly better performance, consistent with the statistical results of the 19 typhoons. The track errors are 23, 15, and 105 km for BLD and 35, 25, and 129 km for GFS at 12-, 24-, and 36-h forecasts, respectively. The track forecast error difference is less than 30 km over the 36-h forecast period for these two experiments.

The central pressure of the BLD experiment at 0600 UTC 12 July is lower than that from the GFS experiment (i.e., 940 versus 974 hPa in Fig. 11), and is much closer to the observed central pressure of 935 hPa from the best track. A mesoscale vortex with tightly packed isobars and strong winds is quite evident in the surface analysis of BLD. Within this context, the GFS analysis displays a broad typhoon circulation pattern, without the structure of a mesoscale vortex. The winds are weaker, and there are no packed isobars. Clearly, BLD produces a detailed typhoon pressure and wind structure that looks realistic. Associated with the outer circulation

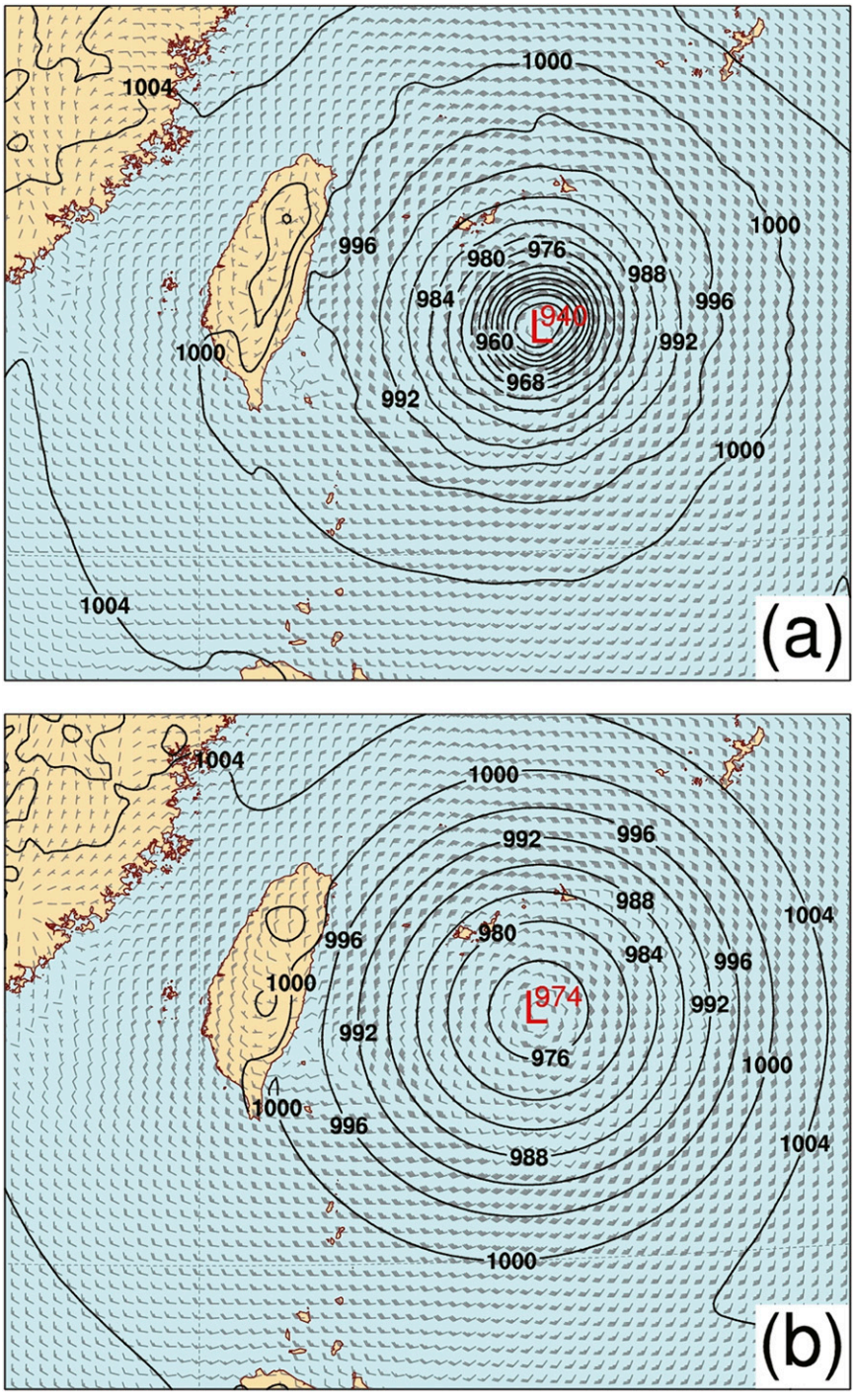

FIG. 11. The sea level pressure analysis and wind vectors [>40 knots (kt; 1 kt = 0.51 m s^{-1}); 1 full barb = 10 kt] from the (a) BLD and (b) GFS experiments at 0600 UTC 12 Jul 2013.

of Typhoon Soulik, strong northerly flow prevails over the ocean to the north of Taiwan in both the GFS and BLD analyses (Fig. 11). However, the flow over the CMR is quite different between these two analyses. As the northerly flow enters Taiwan, it becomes light and variable for BLD. On the other hand, it remains strong and turns persistently westerly for GFS. These differences suggest that the blended analysis better captures the influence of the CMR. The GFS analysis, derived from the NCEP global model, does not experience the

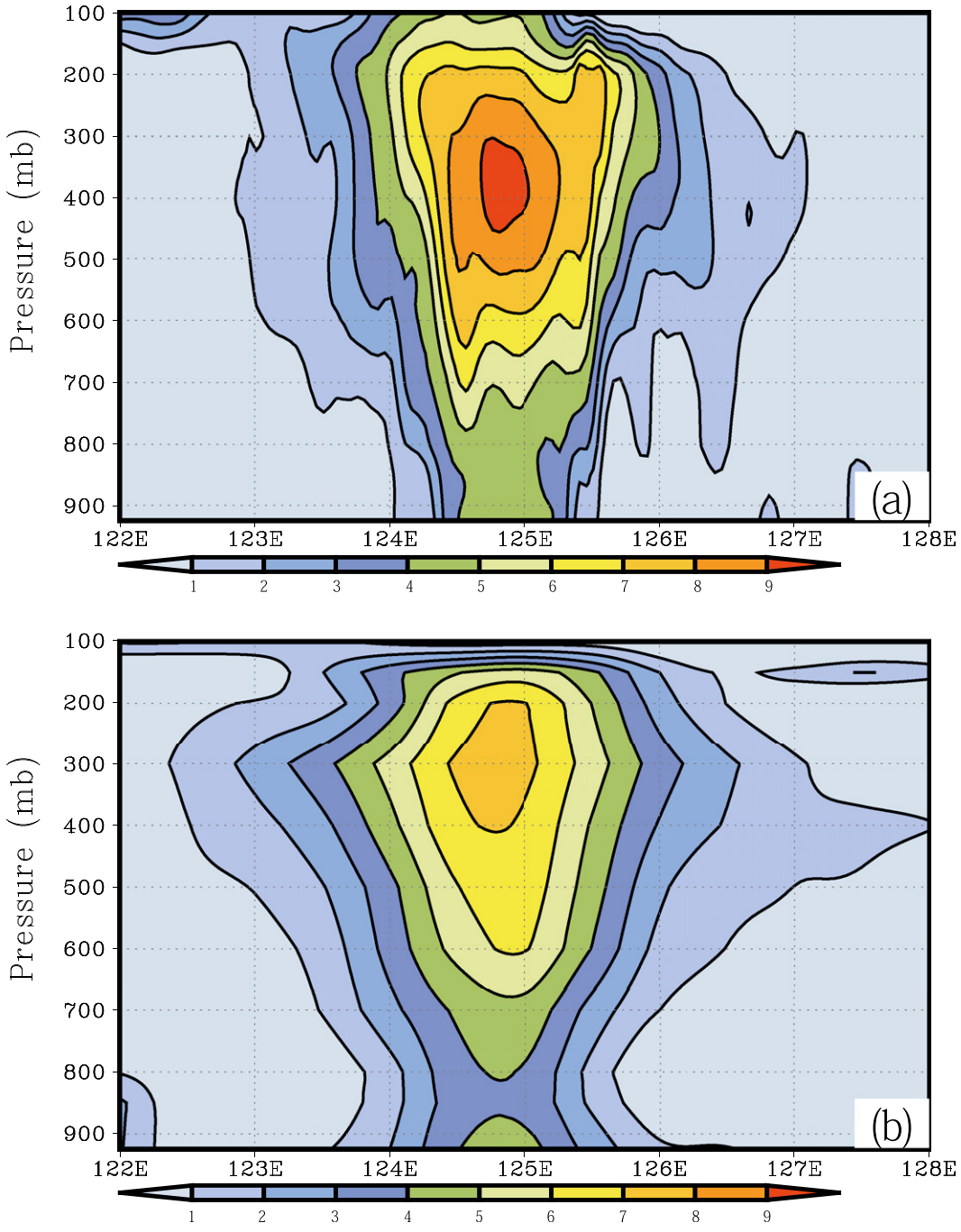

FIG. 12. Zonal cross section of the anomaly temperature (°C) cutting through the typhoon center from the (a) BLD and (b) GFS experiments for the model initial conditions at 0600 UTC 12 Jul 2013.

same level of topographic influence. One possible reason is that the GFS has a much smoother topography compared with the TWRF Model at 5-km resolution. The ability to better capture the topographic effects will help BLD to produce more accurate typhoon circulation patterns in the vicinity of Taiwan.

Figure 12 shows an east–west vertical cross section of the temperature anomaly cutting across the typhoon center for the model initial conditions at 0600 UTC 12 July. A warm core structure is clearly visible with the maximum temperature anomaly exceeding 8°C located at about 350 hPa around the typhoon center in the blended

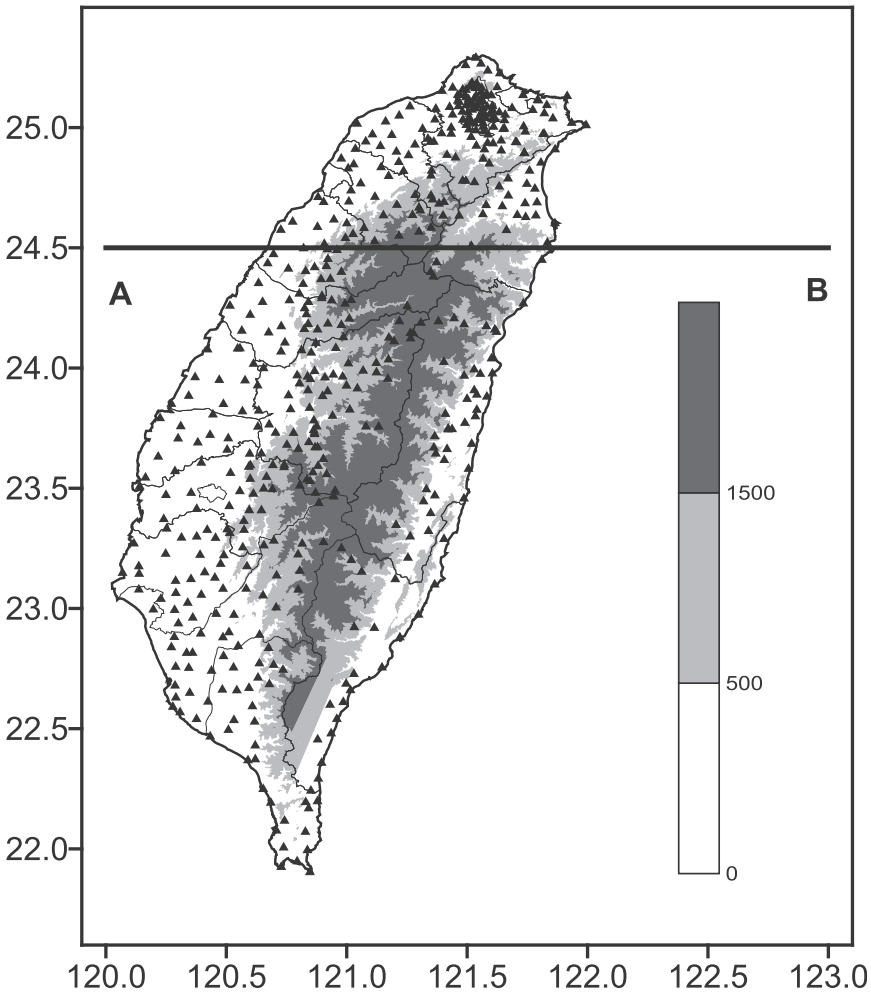

FIG. 13. Taiwan topography with increasing gray shading for 500 and 1500 m. The 512 rainfall stations including conventional, automatic rainfall, and Meteorological Telemetry System stations (triangles) are plotted. Irregular lines indicate the boundaries of 19 counties across Taiwan. Line AB (along 24.5°N, 120°–123°E) is used for cross-sectional analyses in Fig. 12.

analysis. On the contrary, the GFS analysis shows a weaker warm core with much reduced temperature gradients. It is not surprising that the small-scale structures of Typhoon Soulik are not well resolved by the global model. By blending the GFS analysis with the TWRF regional analysis, BLD is able to retain the small-scale features generated by the TWRF Model.

We now verify the rainfall prediction of the BLD and GFS experiments against the observed rainfall obtained from the 512 automatic rain gauge stations across Taiwan (Fig. 13). The maximum 24-h accumulated rainfall produced by Typhoon Soulik was 949 mm in Hsinchu County over the mountainous northwestern area (Fig. 14a). There are also two small rainfall maxima over the central mountain. The forecasts from these two experiments all give the maximum 24-h rainfall at the correct location (Figs. 14b and 14c). However, the maximum rainfall amounts differ by more than 300 mm. The BLD experiment nicely captures the peak rainfall amount of 945 mm and the two small rainfall maxima over central Taiwan. The GFS experiment has the peak rainfall of 629 mm, and fails to capture one of the small rainfall maximums over south-central Taiwan. The superior rainfall forecast by BLD may be attributed to the improved analysis of the typhoon structure, circulation, track, and intensity. With the detailed mesoscale typhoon structure retained in the blended analysis, the model can better capture the topographic effects of the Central Mountain Range and produce a much more accurate rainfall forecast.

To illustrate the importance of upslope motion in producing heavy rainfall, Fig. 15 shows an east–west

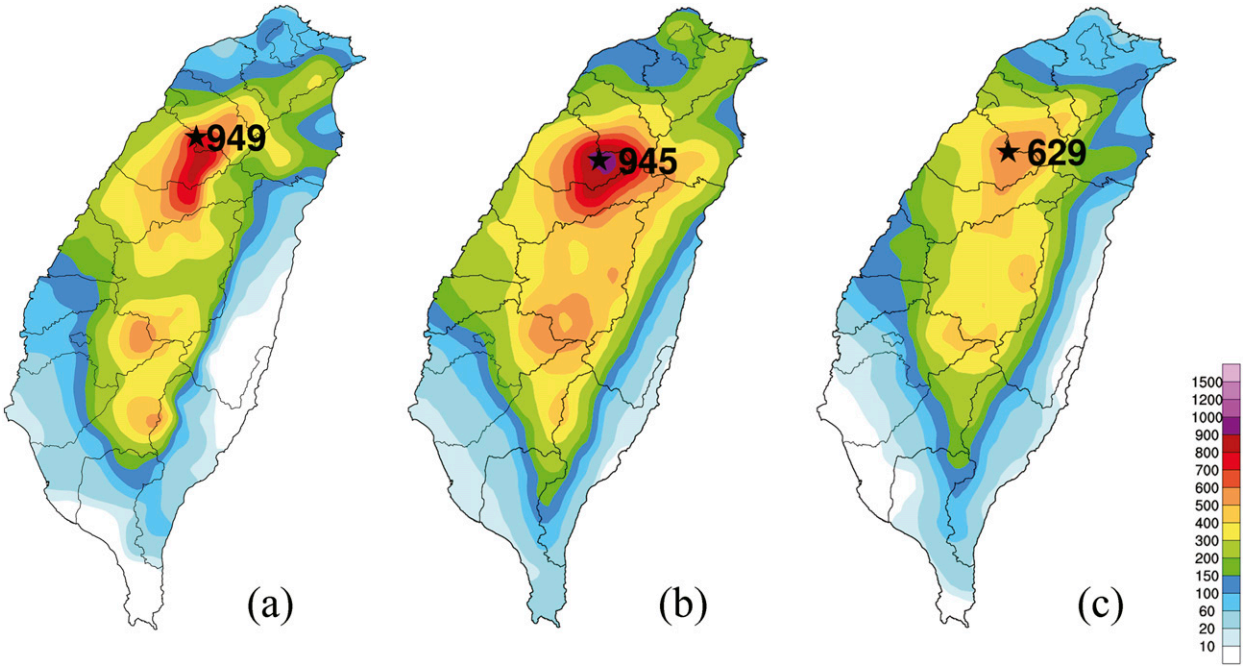

FIG. 14. The 24-h accumulated rainfall (mm) from the forecast initiated at 0600 UTC 12 Jul: (a) observed rainfall, and (b) BLD and (c) GFS experiments.

vertical cross section of two-dimensional wind vectors cutting across the CMR along 24.5°N at forecast hour 17 (when the maximum hourly rainfall occurred, as Typhoon Soulik was passing through northern Taiwan). Two-dimensional wind components constructed from the cross section show a significantly stronger westerly flow with the BLD experiment throughout the troposphere to the west of the CMR. The stronger westerly wind component in BLD forces a deep layer of upslope motion on the windward side of the CMR, thus producing a larger rainfall amount than that from the GFS experiment.

4. Conclusions

Taiwan's Central Weather Bureau implemented a Typhoon WRF (TWRF) Model for operational typhoon prediction in 2010. The TWRF Model consists of triple-nested grids at resolutions of 45, 15, and 5 km, respectively. The TWRF employs a partial cycling data assimilation scheme based on the WRF 3DVAR system. The partial cycling begins with a cold start at 12 h prior to the analysis time based on the NCEP GFS analysis. This is followed by two subsequent data assimilation cycles at 6-h intervals using the TWRF forecast as the first guess. The TWRF partial cycling analysis suffers two deficiencies. First, the TWRF does not assimilate satellite radiance observations. Second, with the existence of lateral boundaries, the observations outside the model domain could not influence the analysis within the model domain. Consequently, systematic biases (due to model physics errors) can develop over the ocean and influence the typhoon prediction.

With an objective of improving the initial conditions for TWRF, we adopt the blending scheme of Yang (2005) to merge the NCEP GFS analysis with the TWRF regional analysis at a cutoff length of 1200 km. For circulations with length greater than 1200 km, the blended analysis is increasingly weighted toward the NCEP global analysis. For circulations with lengths less than 1200 km, the blended analysis is increasingly weighted toward the TWRF partial cycling analysis. At the length of 1200 km, these two analyses are weighted evenly. The impact of analysis blending is tested on 19 typhoons over the western Pacific during 2013.

The blended analysis is shown to be superior to either the NCEP GFS analysis or the original TWRF regional analysis. When verified against the independent high-resolution (25 km) ECMWF global analysis, the TWRF regional analysis is shown to possess sizeable systematic errors over the ocean. This systematic error is largely removed in the blended analysis. It is apparent that the TWRF regional analysis suffers significant deficiency on the large scale, which is well remedied by the introduction of the NCEP GFS analysis through blending. Comparison of 279 forecasts on the 45-km grid for the 19

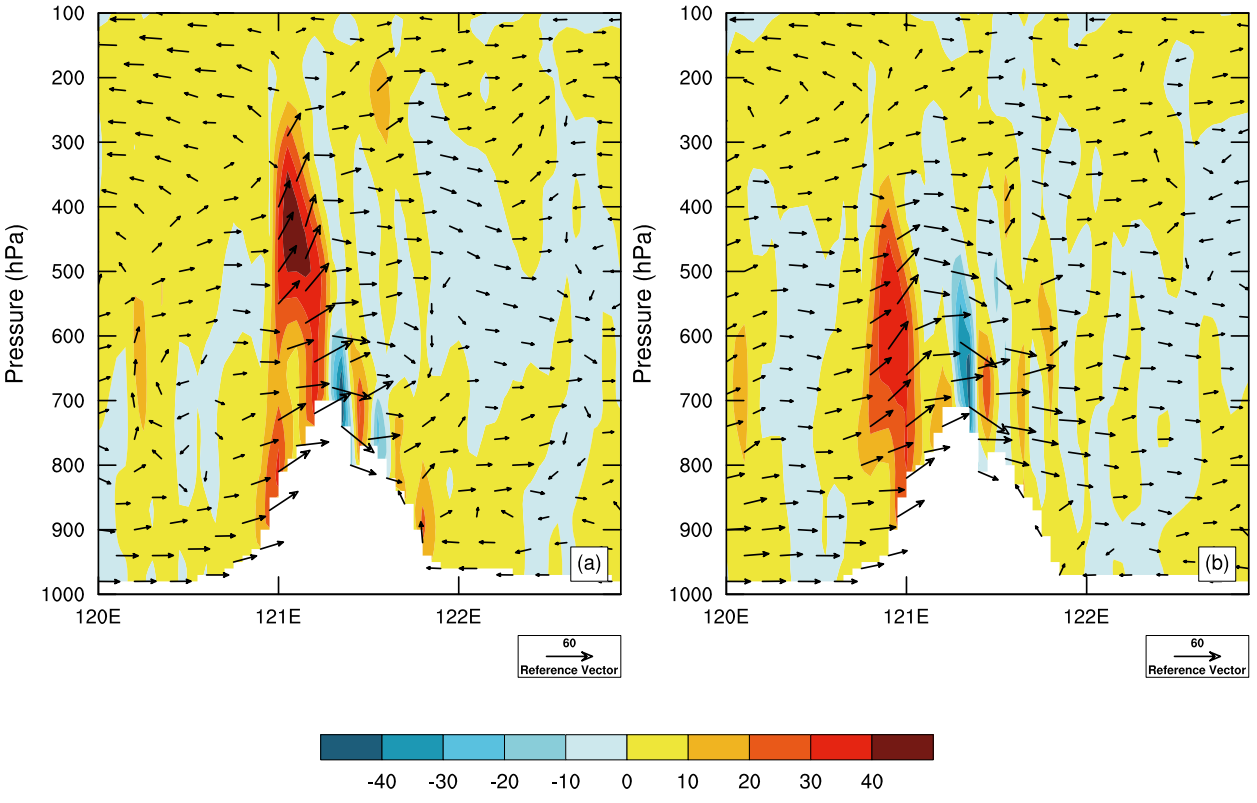

FIG. 15. Zonal cross section (along 24.5°N, 120°–123°E) of two-dimensional wind vectors (u, w; m s^{-1} and Pa s^{-1}, respectively) and vertical velocity (shaded every 1 Pa s^{-1}) at forecast hour 17 (2300 UTC 12 Jul 2013) for the (a) BLD and (b) GFS experiments.

typhoons shows that the TWRF Model initialized with the blended analysis gives a much improved typhoon track forecast. The difference in mean track forecast error, which is statistically significant, can be as big as 80 km in 72-h forecasts, a 30% improvement.

Weighted toward the TWRF regional analysis for scales less than 1200 km, the blended analysis is shown to possess considerably more detailed mesoscale structure than that of the NCEP GFS analysis. For track forecasts on the 15-km grid (where mesoscale analysis is important), TWRF initialized with the blended analysis gives a more accurate track forecast than that initialized with the NCEP GFS analysis. The difference, which is also statistically significant, is about 20 km at 72 h, averaged over 143 cases.

The advantage of the blended analysis over the NCEP GFS analysis is well reflected in the typhoon's wind, temperature, and pressure structure at the model initial conditions, as well as in rainfall prediction on the 5-km grid over Taiwan. Using Typhoon Soulik as an example, which was the only typhoon that made landfall over Taiwan during 2013, we showed that the cycling analysis using a TWRF forecast as the first guess clearly has its advantages in capturing the mesoscale vortex wind and pressure structure at the surface associated with the typhoon circulation as well as the local topographically induced circulations. The detailed mesoscale structure retained in the blended analysis, which includes a mesoscale vortex circulation, a robust warm core, and a stronger upslope flower, led to a much more accurate rainfall forecast both in terms of peak rainfall amount and rainfall distribution. Verification of the rainfall forecast composite from five typhoons that produce rainfall over Taiwan also shows that BLD gives better rainfall forecasts than GFS, consistent with the case study of Typhoon Soulik.

Our study shows that the blended analysis indeed offers the best of both worlds. On one hand, it takes advantages of the superior large-scale fields from the NCEP GFS analysis. This significantly reduces the systematic errors over the ocean and greatly improves the track forecast. On the other hand, it takes advantages of the detailed mesoscale structure associated with the tropical cyclone and the topographic forcing provided by the TWRF partial cycling analysis. This improves the track forecast on the 15-km grid, as well as producing a much more accurate rainfall forecast on the 5-km grid over Taiwan.

The use of the blending method requires very modest additional computation after WRF 3DVAR analysis. It

amounts to less than a 1-min wall-clock time difference with a single-processor Fijitsu supercomputer. With the encouraging results and minimal extra computational cost, the blended analysis is recommended for operational implementation with TWRF at the Central Weather Bureau starting in 2014.

Acknowledgments. This study was supported by the National Science Council of the ROC under Grants NSC99-2625-M-052-003-MY3 and NSC101-2625-M-492-002, the American Institute in Taiwan under Award CWB05-071-119, and the U.S. National Science Foundation under Cooperative Agreement AGS-1033112. YHK acknowledges the support of the NOAA Hurricane Forecast Improvement Project through the Developmental Testbed Center.

REFERENCES

Ajjaji, R., and S. Issara, 1994: Introduction de l'analyse CANARI du modèle global Arpège dans le modèle à domaine limité Aladin. M.S. thesis, Department of Science in Meteorology, École nationale de la météorologie, Toulouse, France, 25 pp. [Available from École nationale de la météorologie, 42 Ave. Coriolis, 31057 Toulouse, France.]

Anthes, R. A., 1982: *Tropical Cyclones: Their Evolution, Structures and Effects. Meteor. Monogr.,* No. 41, Amer. Meteor. Soc., 208 pp.

Barker, D. M., W. Huang, Y.-R. Guo, A. J. Bourgeois, and Q. N. Xiao, 2004: A three-dimensional variational data assimilation system for MM5: Implementation and initial results. *Mon. Wea. Rev.,* **132,** 897–914, doi:10.1175/1520-0493(2004)132<0897:ATVDAS>2.0.CO;2.

Brožkovà, R., and Coauthors, 2001: DFI blending: An alternative tool for preparation of the initial conditions for LAM. *Research Activities in Atmospheric and Oceanic Modelling,* H. Ritchie, Ed., WMO CAS/JSC WGNE Rep. 31, 1.7–1.8.

Chan, J. C. L., and W. M. Gray, 1982: Tropical cyclone movement and surrounding flow relationships. *Mon. Wea. Rev.,* **110,** 1354–1376, doi:10.1175/1520-0493(1982)110<1354:TCMASF>2.0.CO;2.

Chen, F., and J. Dudhia, 2001: Coupling an advanced land-surface–hydrology model with the Penn State–NCAR MM5 modeling system. Part I: Model description and implementation. *Mon. Wea. Rev.,* **129,** 569–585, doi:10.1175/1520-0493(2001)129<0569:CAALSH>2.0.CO;2.

Dahlgren, P., and N. Gustafsson, 2012: Assimilating host model information into a limited area model. *Tellus,* **64A,** 15836, doi:10.3402/tellusa.v64i0.15836.

Durand, Y., and P. Bougeault, 1987: L'analyse objective PERIDOT. Note de travail 193, Direction de la Météorologie Nationale/EERM, 193 pp.

Guidard, V., and C. Fischer, 2008: Introducing the coupling information in a limited-area variational assimilation. *Quart. J. Roy. Meteor. Soc.,* **134,** 723–736, doi:10.1002/qj.215.

Hendricks, E. A., M. S. Peng, and T. Li, 2013: Evaluation of multiple dynamic initialization schemes for tropical cyclone prediction. *Mon. Wea. Rev.,* **141,** 4028–4048, doi:10.1175/MWR-D-12-00329.1.

Hong, S.-Y., Y. Noh, and J. Dudhia, 2006: A new vertical diffusion package with an explicit treatment of entrainment processes. *Mon. Wea. Rev.,* **134,** 2318–2341, doi:10.1175/MWR3199.1.

Hsiao, L. F., C. S. Liou, T. C. Yeh, Y. R. Guo, D. S. Chen, K. N. Huang, C. T. Terng, and J. H. Chen, 2010: A vortex relocation scheme for tropical cyclone initialization in Advanced Research WRF. *Mon. Wea. Rev.,* **138,** 3298–3315, doi:10.1175/2010MWR3275.1.

——, D. S. Chen, Y. H. Kuo, Y. R. Guo, T. C. Yeh, J. S. Hong, C. T. Fong, and C. S. Lee, 2012: Application of WRF 3DVAR to operational typhoon prediction in Taiwan: Impact of outer loop and partial cycling approaches. *Wea. Forecasting,* **27,** 1249–1263, doi:10.1175/WAF-D-11-00131.1.

——, and Coauthors, 2013: Ensemble forecasting of typhoon rainfall and floods over a mountainous watershed in Taiwan. *J. Hydrol.,* **506,** 55–68, doi:10.1016/j.jhydrol.2013.08.046.

Huang, X.-Y., and Coauthors, 2009: Four-dimensional variational data assimilation for WRF: Formulation and preliminary results. *Mon. Wea. Rev.,* **137,** 299–314, doi:10.1175/2008MWR2577.1.

Iacono, M. J., J. S. Delamere, E. J. Mlawer, M. W. Shephard, S. A. Clough, and W. D. Collins, 2008: Radiative forcing by long-lived greenhouse gases: Calculations with the AER radiative transfer models. *J. Geophys. Res.,* **113,** D13103, doi:10.1029/2008JD009944.

Kain, J. S., and J. M. Fritsch, 1990: A one-dimensional entraining/detraining plume model and its application in convective parameterization. *J. Atmos. Sci.,* **47,** 2784–2802, doi:10.1175/1520-0469(1990)047<2784:AODEPM>2.0.CO;2.

Liu, Z., C. S. Schwartz, C. Snyder, and S.-Y. Ha, 2012: Impact of assimilating AMSU-A radiances on forecasts of 2008 Atlantic tropical cyclones initialized with a limited-area ensemble Kalman filter. *Mon. Wea. Rev.,* **140,** 4017–4034, doi:10.1175/MWR-D-12-00083.1.

Mlawer, E. J., S. J. Taubman, P. D. Brown, M. J. Iacono, and S. A. Clough, 1997: Radiative transfer for inhomogeneous atmosphere: RRTM, a validated correlated-*k* model for the longwave. *J. Geophys. Res.,* **102,** 16 663–16 682, doi:10.1029/97JD00237.

Raymond, W. H., and A. Garder, 1991: A review of recursive and implicit filters. *Mon. Wea. Rev.,* **119,** 477–495, doi:10.1175/1520-0493(1991)119<0477:ARORAI>2.0.CO;2.

Schwartz, C. S., and Z. Liu, 2014: Convection-permitting forecasts initialized with continuously cycling limited-area 3DVAR, ensemble Kalman filter, and "hybrid" variational–ensemble data assimilation systems. *Mon. Wea. Rev.,* **142,** 716–738, doi:10.1175/MWR-D-13-00100.1.

Skamarock, W. C., and Coauthors, 2008: A description of the Advanced Research WRF version 3. NCAR Tech. Note NCAR/TN-475+STR, 113 pp. [Available online at http://www2.mmm.ucar.edu/wrf/users/docs/arw_v3.pdf.]

Tao, W.-K., and Coauthors, 2003: Microphysics, radiation and surface processes in the Goddard Cumulus Ensemble (GCE) model. *Meteor. Atmos. Phys.,* **82,** 97–137, doi:10.1007/s00703-001-0594-7.

Wang, X., D. Parrish, D. Kleist, and J. Whitaker, 2013: GSI 3DVar-based ensemble–variational hybrid data assimilation for NCEP Global Forecast System: Single-resolution experiments. *Mon. Wea. Rev.,* **141,** 4098–4117, doi:10.1175/MWR-D-12-00141.1.

Wilks, D. S., 1997: Resampling hypothesis tests for autocorrelated fields. *J. Climate,* **10,** 65–82, doi:10.1175/1520-0442(1997)010<0065:RHTFAF>2.0.CO;2.

Yang, X., 2005: Analysis blending using a spatial filter in grid-point model coupling. *HIRLAM Newsletter,* No. 48, Article 10, HIRLAM Programme, de Bilt, Netherlands, 49–55. [Available online at http://www.hirlam.org/index.php/meeting-reports-and-presentations/doc_download/517-hirlam-newsletter-no-48-article10-yang.]